Heliyon 9 (2023) e18121

Contents lists available at ScienceDirect

Heliyon

journal homepage: www.cell.com/heliyon

Dissociation of energy connectivity and functional connectivity in Alzheimer's disease is associated with maintenance of cognitive performance

Jinhua Sheng [a,b,*], Ze Yang [a,b], Qiao Zhang [c,d,e], Luyun Wang [a,b], Yu Xin [a,b]

[a] College of Computer Science and Technology, Hangzhou Dianzi University, Hangzhou, Zhejiang, 310018, China
[b] Key Laboratory of Intelligent Image Analysis for Sensory and Cognitive Health, Ministry of Industry and Information Technology of China, Hangzhou, Zhejiang, 310018, China
[c] Beijing Hospital, Beijing, 100730, China
[d] National Center of Gerontology, Beijing, 100730, China
[e] Institute of Geriatric Medicine, Chinese Academy of Medical Sciences, Beijing, 100730, China

ARTICLE INFO

Keywords:
Alzheimer's disease
Energy connectivity
Functional connectivity
Default mode network
MoCA score

ABSTRACT

The correlation between functional connectivity (FC) network segregation, glucose metabolism and cognitive decline has been recently identified. The coupling relationship between glucose metabolism and the intensity of neuronal activity obtained using hybrid PET/MRI techniques can provide additional information on the physiological state of the brain in patients with AD and mild cognitive impairment (MCI). It is a valuable task to use the above rules for constructing biomarkers that are closely related to the cognitive ability of individuals to monitor the pathological status of patients. This study proposed the concept of the energy connectivity (EC) network and its construction method. We hypothesized that the dissociation between energy connectivity and functional connectivity of brain regions is a valid indicator of cognitive ability in patients with dementia. The number of EC-attenuated brain regions (EC-AR) and the number of FC-attenuated brain regions (FC-AR) are obtained by comparison with the normal group, and the dissociation between functional connectivity and energy connectivity is indicated using the ratio of FC-AR to EC-AR for individuals in the disease group. The findings suggest that FC-AR/EC-AR values are accurate predictors of cognitive performance, while taking into account the cognitive recovery due to compensatory effects of the brain. The cognitive ability of some patients with cognitive recovery can also be predicted more accurately. This also indicates that lower functional connectivity and higher energy connectivity between network modules may be one of the important features that maintain cognitive performance. The concept of energy connectivity also has potential to help explore the pathological state of AD.

1. Introduction

Massive disruption of functional brain networks has been identified in association with the progression of Alzheimer's disease (AD) [1]. In the cerebral cortex, information is processed through interactions between various subregions. Anatomical tract tracing,

* Corresponding author. College of Computer Science and Technology, Hangzhou Dianzi University, Hangzhou, Zhejiang, 310018, China.
E-mail address: j.sheng@ieee.org (J. Sheng).

https://doi.org/10.1016/j.heliyon.2023.e18121
Received 9 December 2022; Received in revised form 19 May 2023; Accepted 7 July 2023
Available online 13 July 2023

connectomics, and electrophysiology are used to infer the organization of brain regions and identify several major brain networks. Each brain network is referred to as a "module", corresponds to a major function, and is composed of a number of brain regions [2]. Among several major brain network modules, the default mode network (DMN) is considered one of the core network modules, and its function is closely related to situational memory and cognitive abilities. Using functional magnetic resonance imaging (fMRI) techniques, it is found that the DMN of AD patients all exhibited significant functional impairment and abnormal organization [3]. As the severity of AD increases, there is a substantial loss of intra-network connectivity and inter-network anti-correlation [1]. Some investigators found increased network connectivity between the salience network (SN) and DMN in patients with MCI and AD, suggesting a disruption of the SN-centered network model [4].

Recently, there has been an increasing interest in combining fMRI and PET imaging to explore the relationship between functional network abnormalities and glucose metabolism. [^{18}F]-Fluorodeoxyglucose (FDG) is a radioactive contrast agent that provides information about the metabolism of glucose in an organism. When FDG is injected into the body, it accumulates in areas with a high metabolic rate and exhibits a high FDG-standardized uptake value ratio (FDG-SUVR). Some scholars have suggested that glucose metabolism disorder is one of the important characteristics of AD, and the relationship is increasingly close [5,6]. Prototypical glucose metabolism alterations are also observed in patients with amnestic mild cognitive impairment (MCI) [7,8]. As AD progresses, both functional brain network segregation and glucose metabolism decrease and associated with cognitive decline [9]. Intra- and inter-network connectivity is critical for achieving the optimal "trade-off" between minimizing energy consumption and maximizing functional efficiency in the normal brain [10]. Connectivity between the whole brain network modules is associated with cognitive performance [11], and FDG-SUVR may also be used as a proxy indicator of cognitive performance. These findings further elucidated that abnormalities in metabolic and functional connectivity may underlie the neural basis of cognitive dysfunction in AD [12]. In addition to the level of glucose metabolism, the intensity of neuronal synaptic activity is also reflected in the power spectrum [12]. The amplitude of low frequency fluctuation (ALFF) reveals the intensity of the blood oxygenation level dependent (BOLD) signal for regional spontaneous activity and can indicate the strength of neuronal activity in different brain regions, thus exploring the hidden neurophysiological significance of this activity. The ALFF represents the intensity of neuronal activity, and if low-frequency signal fluctuations are more consistent between brain regions, it may indicate that they have similar functions (higher functional connectivity). It has been shown that the correlation between FDG-SUVR and the ALFF is closely related to cognitive performance [13].

Combining the MCI and AD stages in research could lead to better understanding of the progression of dementia, which could improve the outcome of treatments. Studies have shown that abnormal cerebral metabolic rate of glucose and energy generation in specific brain regions are one of the early characteristic changes of AD, and have indicated that the abnormal metabolism of glucose is the early manifestation of AD [14].

It would be valuable to investigate the relationship between these characteristics and how to integrate the information from these brain networks to find markers that more accurately describe the cognitive abilities and pathological states of patients. We constructed generalized linear regression models based on the sex and age of the individuals in the normal group, and screened the brain regions with weaker metrics (FDG-SUVR, ALFF) in the disease group for subsequent studies. In this study, we proposed an energy information network constructed based on FDG-SUVR and ALFF. The ratio of the number of brain regions with weak functional connectivity and the number of brain regions with weak energy information coherence is closely related to MoCA scores and can be an important predictor of cognitive ability. And this method is found to reflect, to a certain extent, the cognitive recovery due to compensatory effects. The schematic diagram of the energy connection is shown in Fig. 2. The overall process of the study is shown in Fig. 1.

2. Materials and methods

All PET and MRI image data is downloaded from the AD Neuroimaging Initiative (ADNI) database (http://adni.loni.usc.edu). Data

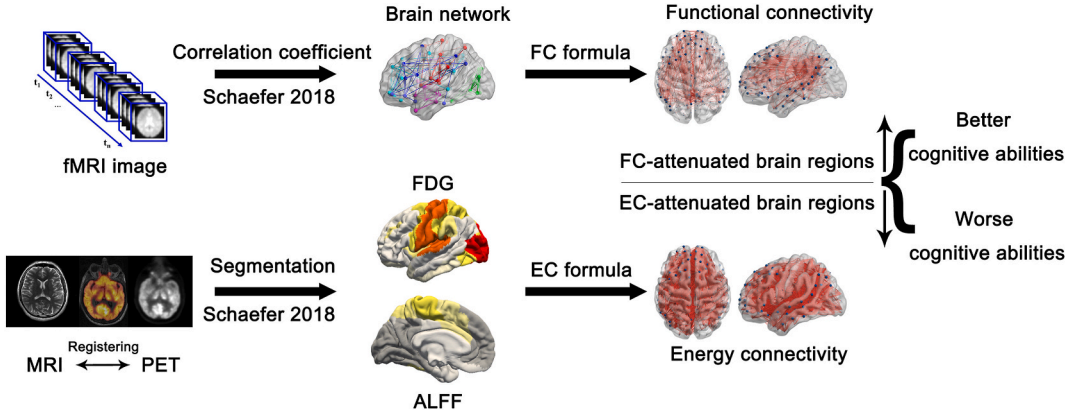

Fig. 1. Research methods and data processing flowchart. PET-MRI : Courtesy of Dr. Theberge, Lawson Research Institute, London, ON, Software version VB20P. fMRI : https://developer.nvidia.com/blog/nvidia-digits-alzheimers-disease-prediction/.
Other images from BrainNet viewer and Freesurfer.

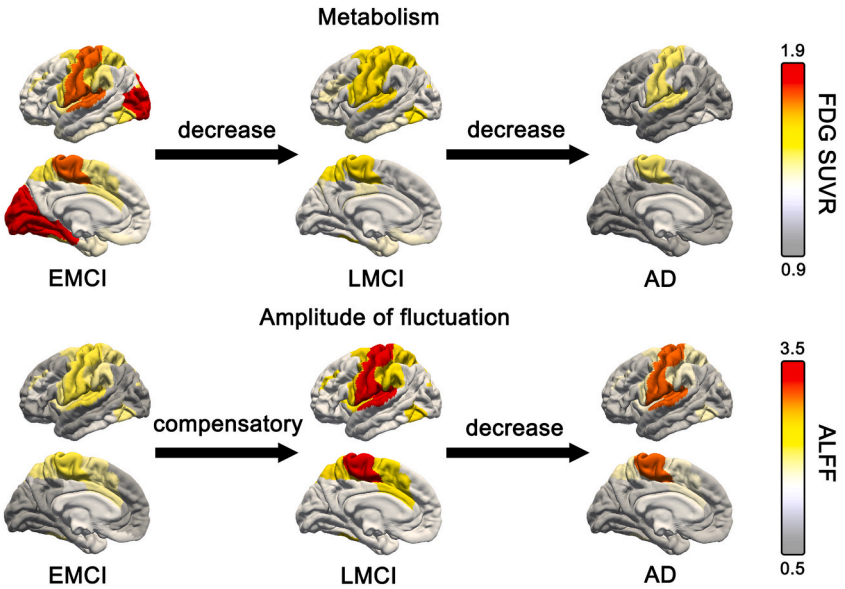

Fig. 2. Schematic representation of the relationship between glucose metabolism and amplitude of low frequency fluctuations. ALFF increases before the onset of rigid dementia as a result of a compensatory mechanism.

collection and sharing for this project is funded by the ADNI database. Informed consent is obtained from the volunteer in accordance with the institutional review board policy. All methods are carried out in accordance with relevant guidelines and regulations. All experimental protocols were approved by the Institutional Review Board (IRB) at Hangzhou Dianzi University (IRB-2020001) and the Ethics Committee at Beijing Hospital (2022BJYYEC-375-01).

2.1. Subjects

Demographic information about the subjects is shown in Tables 1 and 2. Two hundred and fifteen individuals with [^{18}F]-Fluorodeoxyglucose PET, functional magnetic resonance imaging (fMRI) and T1-weighted structural MRI images from the Alzheimer's Disease Neuroimaging Initiative (ADNI) are included in this study. Among them, the experimental dataset has 133 participants, including 41 cognitively normal (CN) participants, 32 patients with EMCI, 31 patients with LMCI, and 29 patients with AD. The validation dataset has 82 participants, including 17 cognitively normal (CN) participants, 24 patients with EMCI, 17 patients with LMCI, and 24 patients with AD. This study selected participants from the ADNI database (http://adni.loni.usc.edu) who had 18F-FDG PET and fMRI scans less than one month apart. Each subject is examined by the Montreal Cognitive Assessment (MoCA), Mini-Mental State Examination (MMSE), and global clinical dementia rating (CDR >0.5 for AD diagnosis). Patients are followed up with cognitive ability tests every six months or a year. We excluded individuals with a greater difference between the time of cognitive ability diagnosis and the time of image scanning. ADNI studies are conducted in accordance with the Good Clinical Practice guidelines, the Declaration of Helsinki, and U.S. 21 CFR Part 50 (Protection of Human Subjects), and Part 56 (Institutional Review Boards). This study is approved by the Institutional Review Boards of all of the participating institutions. Informed written consent is obtained from all participants at each site.

Table 1
Experimental dataset Demographics.

	Health Control (HC)	EMCI	LMCI	AD
N	41	32	31	29
Age	74.1 ± 5.8	74.6 ± 4.4	72.3 ± 5.6	75.0 ± 6.7
Gender, F/M	26/15	17/15	17/14	16/13
MMSE	27.9 ± 1.7	27.3 ± 2.3	26.4 ± 2.2	22.0 ± 2.0
MoCA	23.5 ± 3.0	19.9 ± 2.8	20.7 ± 2.7	16.2 ± 2.7
CDR_global				
0	37 (90.2%)	5 (15.6%)	0	0
0.5	4 (9.8%)	23 (71.9%)	29 (93.5%)	10 (34.5%)
1	0	4 (12.5%)	2 (6.5%)	18 (62.1%)
2	0	0	0	1 (3.4%)

Table 2
Validation dataset Demographics.

	HC	EMCI	LMCI	AD
N	17	24	17	24
Age	74.9 ± 6.6	71.0 ± 5.0	71.8 ± 6.3	73.6 ± 6.3
Gender, F/M	9/8	13/11	7/10	11/13
MMSE	28.5 ± 1.3	28.3 ± 1.3	27.3 ± 2.0	23.3 ± 1.8
MoCA	26.0 ± 2.2	22.1 ± 3.9	21.4 ± 2.0	19.9 ± 2.9
CDR_global				
0	15 (88.2%)	0	0	0
0.5	1 (5.9%)	23 (92.0%)	17 (100%)	13 (54.2%)
1	1 (5.9%)	1 (8.0%)	0	11 (45.8%)
2	0	0	0	0

Results are presented as mean ± SD (%); Mini-Mental State Examination (MMSE); Montreal Cognitive Assessment (MoCA); Clinical Dementia Rating Scale (CDR).

2.2. Image processing

MRI, fMRI, and PET acquisition protocols are detailed elsewhere, see www.adni-info.org. The fMRI data are processed using the CONN functional connectivity toolbox software (CONN). First, slice timing correction and head motion correction are performed on the fMRI time series signal. The repetition time of fMRI sampling is 3000 ms. When analyzing fMRI data, a realignment is applied to the time series signal in order to eliminate the effect of motion. To eliminate motion artifacts, the 3D time series images of the same modality in the fMRI data are aligned by using six motion parameters that describe the spatial transformation (three translations and three rotations). All images are aligned to Montreal Neurological Institute (MNI) standard space, with a resampled isotropic spatial resolution of 3 mm. Extraction of 0.01–0.1Hz signal using temporal band-pass filtering to remove low frequency linear drift and high frequency physiological noise such as respiration and heartbeat. Finally, spatial smoothing is performed using an 8 mm FWHM Gaussian kernel. Time series signals of 400 brain partitions are extracted using the Schaefer2018_400Parcels_7Networks mask for constructing the adjacency matrix and calculating ALFF intensity. Validation dataset samples are calculated using the Schaefer2018_1000Parcels_17Networks mask. The fMRI image data in the ADNI2 database is acquired primarily using the Philips imaging protocol, whereas the majority of the fMRI image data in the ADNI3 database is acquired using the Siemens imaging protocol. To ensure the validity of the results, we repeat the experiment using data from different imaging protocols.

The FDG-PET data is processed using the Petsurfer software. We used FreeSurfer to segment and parcellate MRI T1-weighted images and Petsurfer to calculate the [^{18}F]-Fluorodeoxyglucose standardized uptake value ratio for the whole brain. PET images are obtained according to published imaging protocols. We converted FDG SUVR images from the ADNI database to FDG SUVR images based on MRI, and defined the pons as the reference region. All images are segmented and registered using the FreeSurfer and Petsurfer programs. We performed head movement correction on FDG-PET images of all samples to eliminate the deviation caused by head movement in the image process, and all PET images of individuals are aligned to the mean FDG-PET image. Before analyzing the FDG-PET data, the high-resolution segments for running the partial volume effects method are created using the "gtmseg" function in FreeSurfer, and a registration file is generated from the PET image data in NII format. FDG-PET data are corrected for partial volume effects (PVC), co-registered to the corresponding MRI images, and normalized using the deformation parameters defined from the MRI procedure. The pons are used as reference for quantitative scaling of the image data results, and the standardized uptake value ratio is obtained [15]. In order to improve the quality of image data, the surface is smoothed by a Gaussian filter [16], and the smoothed results are aligned to the human brain standard template (fsaverage) for subsequent analysis [17]. FDG analysis is performed using the Schaefer2018_400Parcels_7Networks mask. Regional glucose metabolism and ALFF intensity are calculated as the mean value within the network masks. Validation dataset samples are calculated using the Schaefer2018_1000Parcels_17Networks mask. The details of the templates are in the supplementary material.

2.3. Construction of energy consistency network

A previous study found a significant Spearman correlation between FDG-PET SUVR and ALFF [13]. In particular, the correlation within the DMN network showed a significant downward trend in the AD group compared to the NC group, while no significant differences are found in whole brain regions of the AD group. FC is mainly used to describe the consistency between modules and does not directly describe the changing pattern of neuronal activity intensity between regions. This study proposes a method to construct an energy information connection network using the glucose metabolism information of each brain region and the amplitude of low frequency fluctuations. This formula is used to describe the consistency of neuronal activity intensity between brain regions, reflecting the efficiency of energy information transfer. The core idea of this formula is to use the ratio of FDG-PET SUVR and ALFF to construct the energy correlation network, which is defined as:

$$EC_{s_i,t} = \frac{\sum_{j\in t}^{N_t} \frac{F_i \times F_j \times (A_i + A_j)}{(F_i + F_j) \times A_i \times A_j}}{N_t} \quad (1)$$

where s_i is the i-th brain partition in module s; t is a brain partitions of modules other than the module s; N_t is the number of all the brain partitions in the rest of the modules except for the module s; and F_i represents the SUVR value of glucose metabolism in region s_i within module s; A_i represents the SUVR value of ALFF intensity in region s_i within module s; F_j represents the SUVR value of glucose metabolism in region j within module t. A_j represents the SUVR value of ALFF intensity in region j within module t.

2.4. Inter-network functional connectivity

In the following analysis of functional and energy synergy between network modules [18], the focus will be on the DMN network, which is closely related to cognition to test our hypothesis on EC and FC alterations associated with cognitive impairment. Inter-network connectivity (inter-FC/EC) is used to evaluate synergy between network s_i and t, which is defined as:

$$FC_{s_i,t} = \frac{\sum_{j \in t} Z_{si,j}}{N_t} \tag{2}$$

where s_i is the i-th brain partition in module s; t is a brain partitions of modules other than the module s; N_t is the number of all the brain partitions in the rest of the modules except for the module s; and $Z_{i,j}$ denotes the Fisher's z-transformed correlation coefficient r between region s_i within module s and region j within module t.

2.5. Statistical analysis

All the statistical analyses are carried out using GraphPad Prism software (version 7.0.4, GraphPad Software Corporation). The demographics and clinical characteristics are compared among the three groups using one-way analyses of variance (ANOVA) for the other variables.

To determine the differences in *FCsi* (Eq. (2)) and *ECsi* (Eq. (1)) occurring in the AD, LMCI, and EMCI groups relative to the CN group, we constructed a generalized linear regression model (GLM) model using age and gender of the CN group as covariates and calculated the W-score of the disease group relative to the CN group. W-scores are similar to z-scores [19], but they are adjusted for specific variates [20]. We first performed a vertex-oriented general linear model (GLM) of glucose metabolism and ALFF in the HC group using age and gender as variates. The formula is shown below:

$$\begin{bmatrix} \text{F1} \\ \text{F2} \\ \text{F3} \\ \cdots \\ \text{M1} \\ \text{M2} \\ \text{M3} \\ \cdots \\ \text{Data} \end{bmatrix} = \underbrace{\begin{matrix} \text{F} & \text{M} & \text{F}_{\text{Age}} & \text{M}_{\text{Age}} \\ 1 & 0 & 76 & 0 \\ 1 & 0 & 72 & 0 \\ 1 & 0 & 71 & 0 \\ & & \cdots & \\ 0 & 1 & 0 & 72 \\ 0 & 1 & 0 & 74 \\ 0 & 1 & 0 & 72 \\ & & \cdots & \end{matrix}}_{\text{Design Matrix}} \bullet \begin{bmatrix} \beta_{\text{F}} \\ \beta_{\text{M}} \\ \beta_{\text{F}_{\text{Age}}} \\ \beta_{\text{M}_{\text{Age}}} \\ \text{Regression Coefficients} \end{bmatrix} \tag{3}$$

Eq. (3) is the general linear model, where F represents female and M represents male. The middle part is the design matrix based on the gender and age of each group, and this matrix is used to perform the construction of generalized linear regression models on gender and age, and to construct generalized linear regression models for normal samples for subsequent comparisons. β_{F} is the regression coefficient for females; β_{M} is the regression coefficient for males; $\beta_{\text{F}_{\text{Age}}}$ is the regression coefficient for female age; $\beta_{\text{M}_{\text{Age}}}$ is the regression coefficient for male age. These parameters are all generated based on the standard cerebral cortex.

Next, we used age and gender β-term plots, as well as regression model residual maps, to calculate a vertex-wise W-score of glucose hypometabolism and ALFF for each patient in the EMCI, LMCI, and AD groups. The formula for calculating the w-score is shown below:

$$\text{W} - \text{score} = \frac{\text{Xpatient} - \beta\text{gender} * \text{gender} - \beta\text{age} * \text{age}}{\text{RSD}} \ (\text{Hypometabolism};\ \text{ALFF}) \tag{4}$$

where Xpatient is the patient's observed value, βgender and βage are the predicted parameter based on the healthy control GLM, RSD is the residual standard deviation from the control GLM [21], similar to prior methods [22].

The number of brain regions with W-score less than 0 in the EMCI, LMCI and AD groups is calculated and one-way analysis of covariance (ANCOVA) is performed for each group followed by post hoc two-sample t-test. In addition, we calculate the ratio between the number of reduced brain regions in *FCsi* (Eq. (2)) and *ECsi* (Eq. (1)) compared to the normal group. Correlation analysis is used to explore the associations of FC weakening regions, EC weakening regions and FC weakening regions/EC weakening regions ratio with MoCA scores. $P < 0.05$ is considered to be statistically significant.

3. Results

3.1. Demographic and clinical characteristics

Demographics and clinical information for experimental and validation datasets are listed in Tables 1 and 2. No significant differences are found in age and gender among all groups. Some individuals in the late mild cognitive impairment (LMCI) group had higher MoCA scores than those in the early mild cognitive impairment (EMCI) group.

3.2. ^{18}FDG-PET SUVR and ALFF in dementia

Averaged W-scores (Eq. (4)) of hypometabolism mapping for each pathological stage are shown in Fig. 3A. In the stage of EMCI, hypometabolism mainly concerned the temporal polar, angular gyrus, supramarginal gyrus, inferior temporal gyrus, middle temporal gyrus, fusiform gyrus and posterior cingulate cortex. The W-scores of these regions are basically concentrated in 0.5–1, and the difference is not significant compared with the HC group. The W-scores of posterolateral prefrontal cortex, frontal polar, frontal orbital

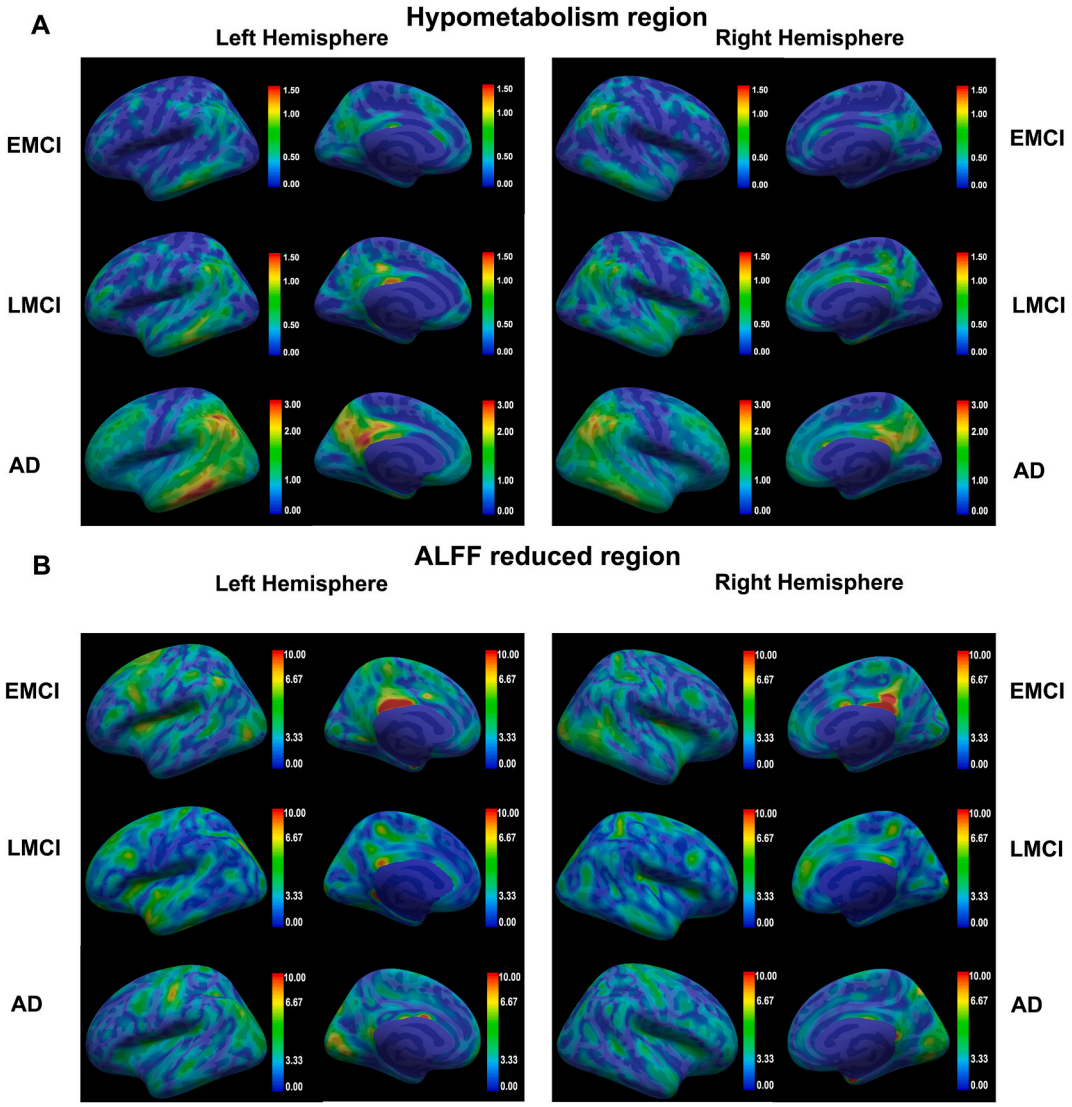

Fig. 3. (A) Representative surface of the average [^{18}F]-Fluorodeoxyglucose standardized uptake value ratio (SUVR) maps in W-score, units compared to HCs, views presented as voxelwise means within each hemisphere. (left-to-right: left lateral, left medial, right lateral, and right medial). (B) Representative surface of the average ALFF maps in W-score, units compared to HCs, views presented as voxelwise means within each hemisphere. (left-to-right: left lateral, left medial, right lateral, and right medial). The W-scores less than 0 of FDG-SUVR and ALFF are obtained by calculating the difference between the true value of each group of individuals and the predicted value of the GLM model constructed based on the sex and age of the CN group. W-scores are taken as absolute values.

and superior lateral frontal cortex increased slightly in the LMCI group. In the patients with AD stage, the W-scores of these regions increased further, temporal polar, angular gyrus, supramarginal gyrus, inferior temporal gyrus, middle temporal gyrus, fusiform gyrus superior and posterior cingulate cortex showed significant differences compared with the HC group.

Averaged W-scores of ALFF mapping for each pathological stage are shown in Fig. 3B. The ALFF significantly decreased with the development of dementia in a large portion of the frontal regions, as well as temporal, occipital lobe regions, demonstrating a reduction in the intensity of local neuronal activity. And these changes are more significant than glucose metabolism. However, by the final stage of AD, the decline in ALLF values subsided, but the degree of hypometabolism is further exacerbated. These results suggested that the correlation between FDG-SUVR and ALFF can reflect the progression of AD, which corresponds to the results of previous studies [13]. Therefore, we proposed constructing an energy correlation network based on this result and assumed that it is closely related to the cognitive ability of individuals.

3.3. *Patterns of EC-AR and FC-AR changes in global brain regions*

The results of global EC and FC changes for experimental dataset are demonstrated in Fig. 4A. Energy connectivity was calculated using Eq. (1), while functional connectivity was calculated using Eq. (2). There is no significant difference in the number of EC-AR in global brain regions among the patients in the three states. As dementia progresses, the number of FC-AR changes more significantly. The number of FC-AR is significantly higher in the EMCI ($p = 0.03$), which are closer in cognitive ability, than in the AD group, indicating that the connectivity between network modules is higher in the AD group than in the MCI group. Previous findings have suggested that impaired segregation of network modules and their decoupling relationship with glucose metabolism are responsible for the cognitive decline in AD [23]. Furthermore, the ratio of FC-AR to EC-AR showed significant changes in some groups, and the FC-AR/EC-AR values in the EMCI group are significantly higher than those in the AD groups ($p = 0.02$), which is consistent with the pattern of changes in the MoCA scores in the demographic information, tentatively indicating a certain association between FC/EC values and cognitive ability. The LMCI group showed higher FC-AR/EC-AR values than the AD group, but did not show significant differences.

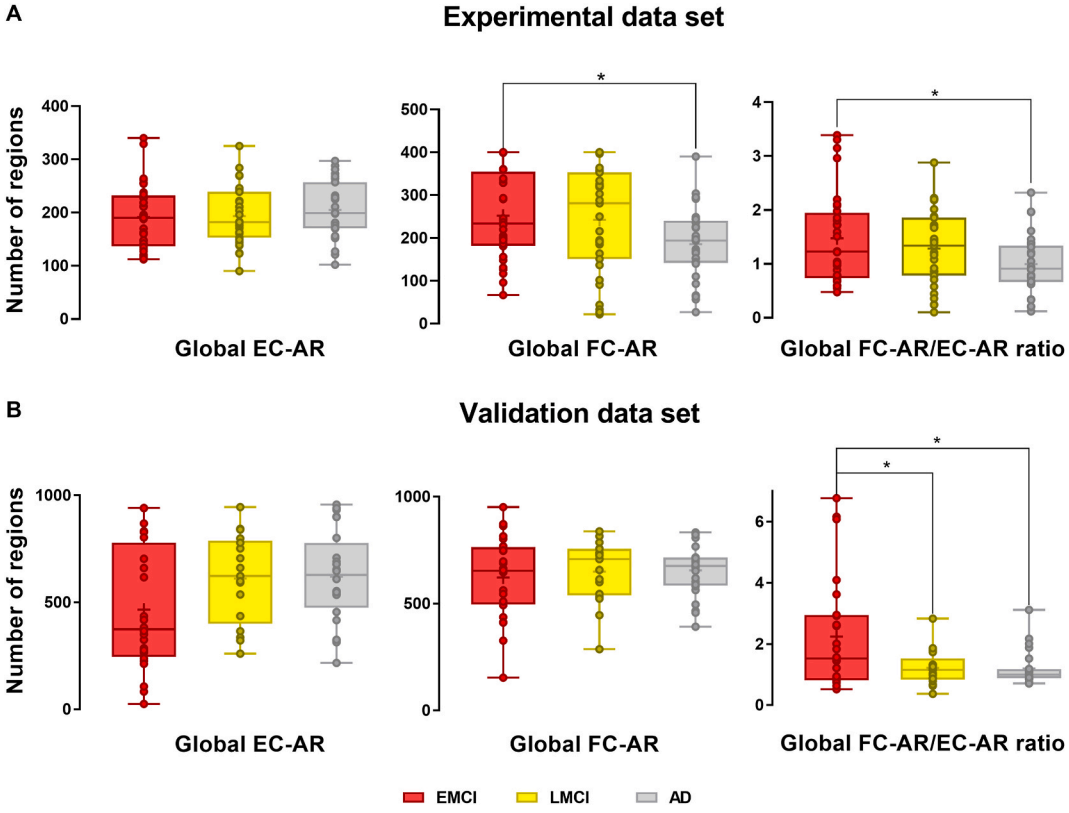

Fig. 4. Patterns of EC-AR and FC-AR changes in global brain regions. (A) Changes in global EC-AR values, global FC-AR values and FC-AR/EC-AR values for individuals in the EMCI, LMCI and AD groups in the experimental dataset. (B) Changes in global EC-AR values, global FC-AR values and FC-AR/EC-AR values for individuals in the EMCI, LMCI and AD groups in the validation dataset. Group differences are compared via GLM analysis with post-hoc two-sample t-tests. *$p < 0.05$. EC-AR and FC-AR are obtained by calculating the difference between the true value of each group of individuals and the predicted value of the GLM model constructed based on the sex and age of the CN group, and EC-AR and FC-AR are the sum of the number of brain regions with W-scores less than 0.

The comparison results of global EC and FC changes for validation dataset are demonstrated in Fig. 4B. To verify that our results are reliable and reproducible, we selected a certain number of samples from the validation dataset for the same analysis. The EC-AR values are lower in the EMCI group than in the LMCI and AD groups. The FC-AR values of the three groups are more consistent. The FC-AR/EC-AR values also showed a similar pattern, which is almost identical to the pattern of MoCA score changes in the demographic information. There is no significant difference in FC-AR/EC-AR values between the LMCI and AD groups. The FC-AR/EC-AR values are also significantly higher in the EMCI group than in the LMCI group and AD group, which is consistent with the change in MoCA scores. Samples are regrouped according to their CDR scores (Fig. 5A and B). Individuals with CDR 1 in the validation dataset had significantly lower global FC-AR/EC-AR values than the CDR 0.5 group ($p < 0.05$, Fig. 5B). Across both data sets, individuals with high CDR scores had lower energy connectivity than individuals with low CDR scores.

3.4. Patterns of EC-AR and FC-AR changes in DMN network

Abnormalities in the DMN network have been found in various psychiatric disorders [24]. DMN is usually associated with self-referential processes and scene memory, and abnormalities in its functional network are the most common presenting symptoms of AD [25]. Based on Eqs. (1) and (2), calculate the energy connectivity and functional connectivity between the DMN network module and other brain regions. There is no significant change in EC-AR values and FC-AR values for the DMN network for the experimental dataset and validation dataset. The number of FC-AR in the DMN network of the experimental dataset changed more significantly compared to the global brain regions. FC-AR values in the LMCI group are higher than those in the EMCI ($p = 0.97$) and AD ($p = 0.17$) groups. There is no significant difference between the EMCI and AD groups. FC-AR/EC-AR values also showed a similar pattern of variation (Fig. 6B), which is consistent with the pattern of cognitive change in the EMCI, LMCI and AD groups.

The results of the comparison of FC-AR/EC-AR values for the three groups of the validation dataset (Fig. 6C) showed significant differences between the EMCI and AD groups ($p = 0.01$). The FC-AR/EC-AR values are also significantly higher in the EMCI group than in the LMCI group ($p = 0.02$), which is consistent with the change in MoCA scores. As shown in Fig. 6A, the DMN network connections are visualized using the BrainNet program. Samples are regrouped according to their CDR scores. Across both data sets, individuals

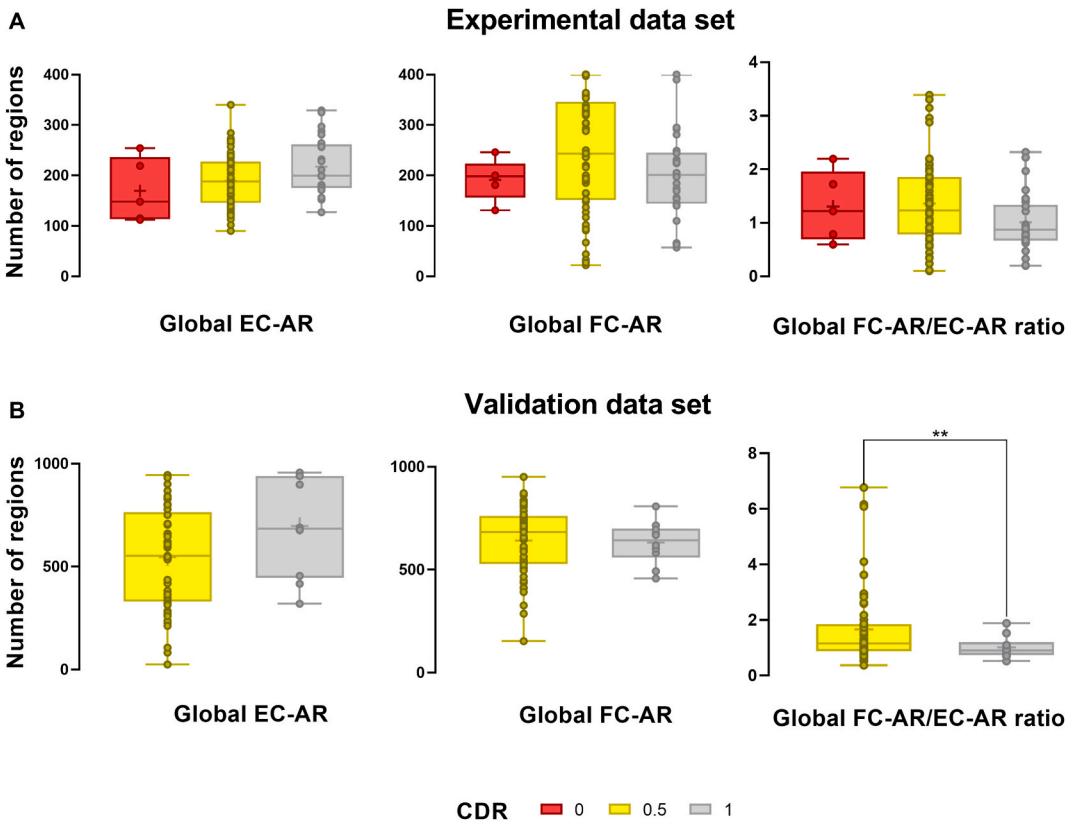

Fig. 5. Patterns of EC-AR and FC-AR changes in global brain regions based on CDR scores. (A) Changes in global EC-AR values, global FC-AR values, and FC-AR/EC-AR values for individuals in the CDR 0, CDR 0.5, and CDR 1 groups in the experimental dataset. (B) Changes in global EC-AR values, global FC-AR values, and FC-AR/EC-AR values for individuals in the CDR 0.5 and CDR 1 groups in the validation dataset. Group differences are compared via GLM analysis with post-hoc two-sample t-tests. *$p < 0.05$; **$p < 0.01$. EC-AR and FC-AR are obtained by calculating the difference between the true value of each group of individuals and the predicted value of the GLM model constructed based on the sex and age of the CN group, and EC-AR and FC-AR are the sum of the number of brain regions with W-scores less than 0.

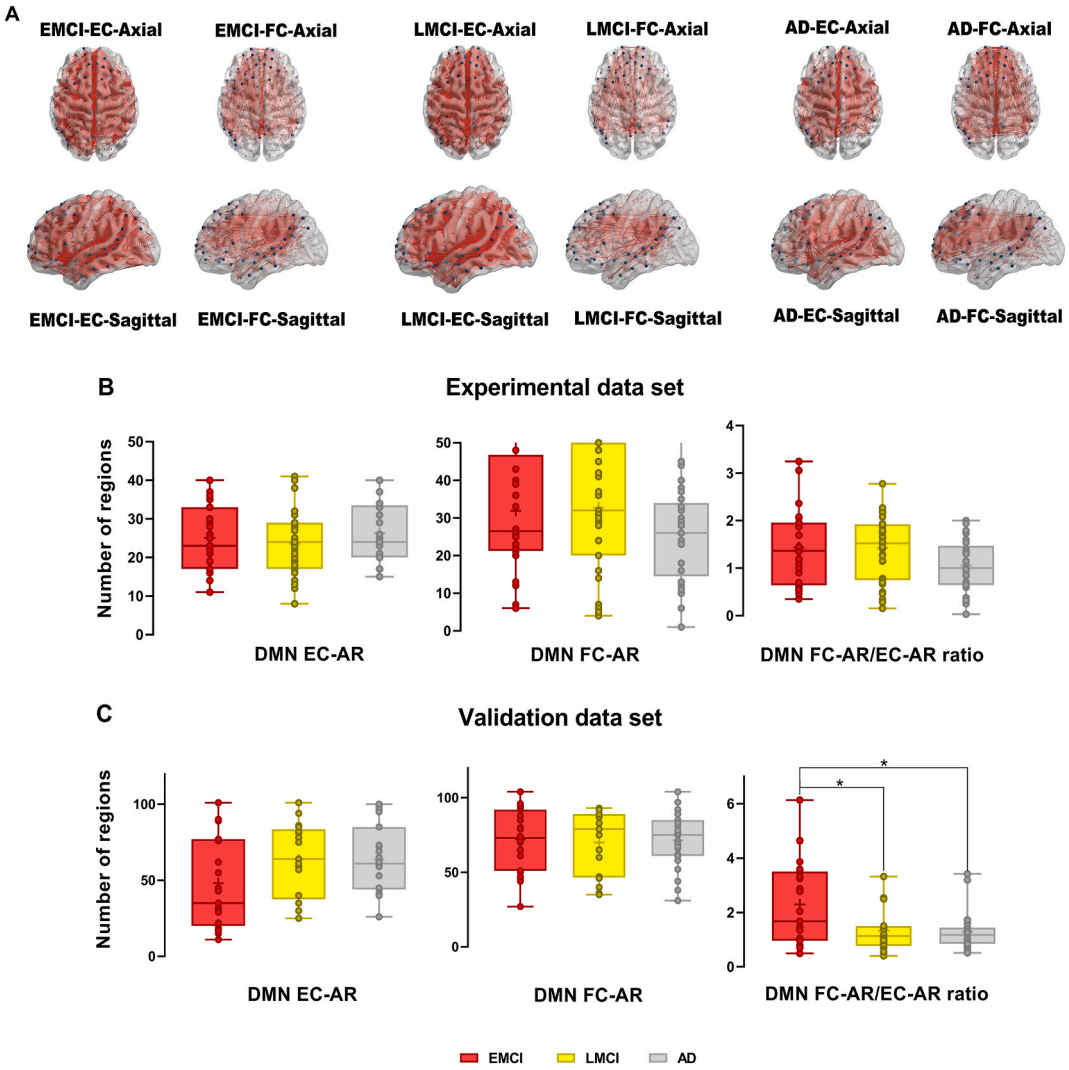

Fig. 6. Patterns of EC-AR and FC-AR changes in DMN network. (A) Visualization of EC and FC network connectivity maps for DMN networks of EMCI, LMCI and AD groups, from both axial and sagittal perspectives. The larger blue dots represent the brain regions inside the DMN network. (B) Changes in DMN network EC-AR values, DMN network FC-AR values and FC-AR/EC-AR values for individuals in the EMCI, LMCI and AD groups in the experimental dataset. (C) Changes in DMN network EC-AR values, DMN network FC-AR values and FC-AR/EC-AR values for individuals in the EMCI, LMCI and AD groups in the validation dataset. Group differences are compared via GLM analysis with post-hoc two-sample t tests. *$p < 0.05$; **$p < 0.01$. EC-AR and FC-AR are obtained by calculating the difference between the true value of each group of individuals and the predicted value of the GLM model constructed based on the sex and age of the CN group, and EC-AR and FC-AR are the sum of the number of brain regions with W-scores less than 0. DMN, Default Mode Network; EC, Energy connectivity; FC, Functional connectivity. (For interpretation of the references to colour in this figure legend, the reader is referred to the Web version of this article.)

with CDR 1 had significantly lower DMN FC-AR/EC-AR values than individuals with CDR 0.5 ($p < 0.05$, $p < 0.01$, Fig. 7A and B). It is found that individuals with high CDR scores also had lower DMN energy connectivity than individuals with low CDR scores in both data sets.

3.5. Correlations between FC-AR/EC-AR values and the MoCA scores

Significant correlations between FC-AR/EC-AR values and MoCA scores of the DMN network module in the EMCI ($p = 0.0001$), LMCI ($p = 0.01$) and AD ($p = 0.0009$) groups in the experimental dataset (Fig. 8A). The validation dataset for the EMCI ($p = 0.0056$), LMCI ($p = 0.025$) and AD ($p = 0.028$) groups also showed almost the same pattern, except for a slight decrease in the significance of the correlation between FC-AR/EC-AR values and MoCA scores (Fig. 8B). The correlation between FC-AR/EC-AR values and MoCA scores decreased with the development of dementia, probably due to the effect of toxic proteins. To further validate the experimental results, we obtained MoCA scores for multiple time points (three follow-up results) for the experimental and validation dataset samples. The

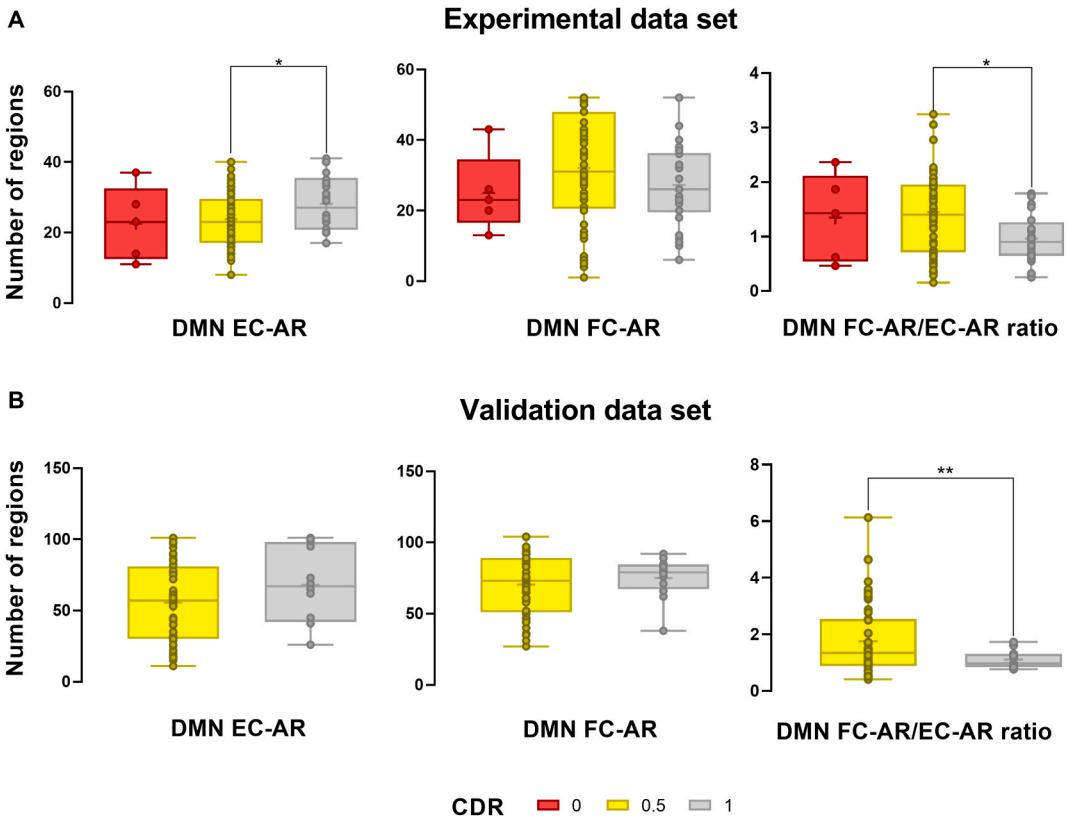

Fig. 7. Patterns of EC-AR and FC-AR changes in DMN network based on CDR scores. (A) Changes in DMN network EC-AR values, DMN network FC-AR values and FC-AR/EC-AR values for individuals in the CDR 0, CDR 0.5, and CDR 1 groups in the experimental dataset. (B) Changes in DMN network EC-AR values, DMN network FC-AR values and FC-AR/EC-AR values for individuals in the CDR 0.5 and CDR 1 groups in the validation dataset. Group differences are compared via GLM analysis with post-hoc two-sample t tests. *$p < 0.05$; **$p < 0.01$. EC-AR and FC-AR are obtained by calculating the difference between the true value of each group of individuals and the predicted value of the GLM model constructed based on the sex and age of the CN group, and EC-AR and FC-AR are the sum of the number of brain regions with W-scores less than 0. DMN: Default Mode Network; EC: Energy connectivity; FC: Functional connectivity.

relationship between the FC-AR/EC-AR values and their corresponding multi-time point results is explored (Fig. 9A and B). As the FC-AR/EC-AR values of the experimental (Fig. 9A) and validation datasets (Fig. 9B) increased, the mean values of the multi-time-point results also improved. But overall, it shows a fluctuating change. Correlation analysis of global network based on FC-AR/EC-AR values and MoCA scores for the validation dataset is presented in Supplementary Material Fig. S2. The results of the validation dataset with multiple time points of MoCA scores are presented in Supplementary Material Fig. S1. Most of the follow-up records for the AD group are recorded only once and are not shown in Fig. S1.

4. Discussion

For the first time, we propose that the concept of energy connectivity be used to represent the similarity in the ability of synapses in different brain regions to transmit signals. By using the default mode network as a seed module, we calculated the functional and energy connection strengths between the DMN module and other modules. The separation between the energy connectivity network and the functional connectivity network constituted by brain regions is more closely related to the maintenance of individual cognitive abilities. We also examined the validation dataset using different masks and are able to accurately predict the cognitive performance of individuals with cognitive recovery. These results have important implications for the clinical diagnosis and assessment of Alzheimer's disease, and have further improved researchers' understanding of the progression of dementia.

The classification of cognitive impairment (EMCI, LMCI) provides a wide window of time for early intervention in Alzheimer's disease and the study of disease progression patterns. Researchers have recently focused their attention on the coupling between neuronal activity and functional connectivity between brain regions, and their correlation could serve as additional information on the physiological state of the brain in patients with dementia [13,26]. The coupling between regional neural activity and topology metrics of inter-module FC has been explored. In MCI and AD, FDG-SUVR and inter-regional FC metrics are disrupted. In addition, AD modified the relationship between FDG-SUVR and inter-regional FC measurements. It is demonstrated that AD attenuates the intensity of regional neural activity and the degree of functional separation in particular brain regions [26]. Another study showed a decrease in

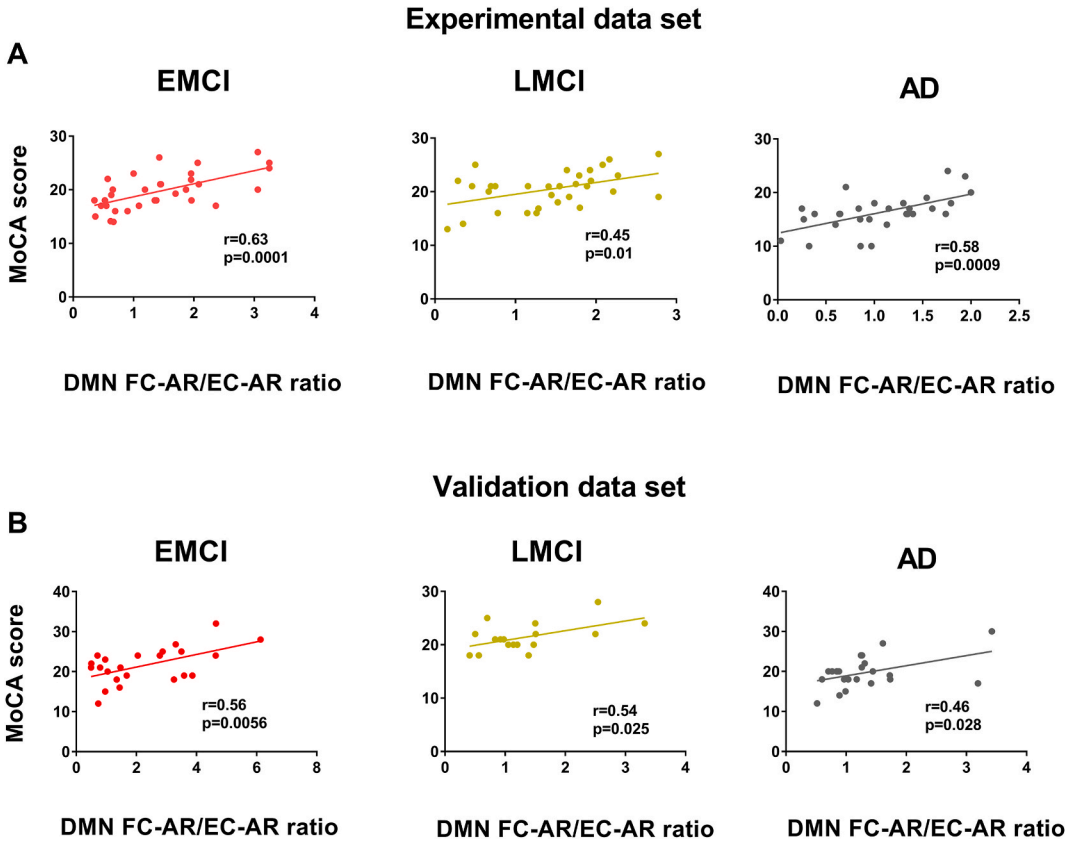

Fig. 8. Correlation analysis of each group based on the DMN network module. (A) Correlation analysis between FC-AR/EC-AR values and MoCA scores of individuals in the experimental dataset. (B) Correlation analysis between FC-AR/EC-AR values and MoCA scores of individuals in the validation dataset. All analyses are performed using Pearson correlation analysis, with p-values representing the degree of significance of the correlation, two-tailed. *p < 0.05; **p < 0.01; ***p < 0.001.

the correlation of FDG-SUVR/fALFF and SUVR/Regional Homogeneity (ReHo) in global brain regions in the preAD group compared to the NC group, and this difference is further amplified in the AD group [13]. Our study is mainly based on the pattern between the level of glucose metabolism and the amplitude of low-frequency oscillations of neuronal activity signals obtained from the above study, and we proposed a method to construct an energy information correlation network. The above two attributes are integrated into a formula and combined with the brain network constructed by fMRI signals to explore the changing patterns of brain pathological states during the development of dementia and suggested a brain network marker that can predict individual cognitive ability more accurately. As shown in Fig. 4A, the global connectivity of all network modules in the LMCI group of the experimental dataset is weaker than in the EMCI and AD groups, and differs more from the AD group. This is generally consistent with the results of another study [23]. And this is consistent with the pattern of MoCA score changes in each group. The FC-AR/EC-AR values in Fig. 4B of the validation dataset showed a similar pattern of change to the MoCA score, with significantly higher values in the EMCI group than in the LMCI and AD groups. MoCA scores are also higher in the EMCI group than in the LMCI and AD groups in the validation data set. The patterns of change in FC-AR/EC-AR values in global brain regions and MoCA scores for the experimental and validation datasets remained basically consistent, but the correlations seemed to be blurred, so we conducted further studies for particular brain network modules.

The DMN module is the network most susceptible to amyloid accumulation [27]. Therefore, a common hypothesis is that the DMN network module region is the preferred target for ad-related pathological processes, including Aβdeposition [27]. The correlation between FDG-SUVR and ReHo values in the DMN network gradually decreases with the increasing accumulation of amyloid [13]. The precuneus and posterior cingulate gyrus are considered to be critical nodes in the DMN network and are highly susceptible to various pathological changes [28]. The FDG-SUVR in the DMN network gradually uncouples from the FC, and the degree of this uncoupling correlates with amyloid load. The researchers concluded that "FDG-FC" coupling" is the only significant variable predicting cognitive status in early and late stage MCI and AD patients [29]. On the other hand, AD has a detrimental effect on the normal coupling of FDG-SUVR and node separations in DMN networks [26].

As shown in Fig. 6A and B, our study showed that the conclusions previously obtained based on global brain regions are further validated when focusing the analyzed subjects on the DMN network from the whole brain level. The decrease in EC network connectivity is more pronounced in the AD group for the experimental and validation datasets. The FC-AR/EC-AR values are higher in the LMCI group than in the EMCI and AD groups for the experimental dataset. This is more consistent with the changing pattern of MoCA

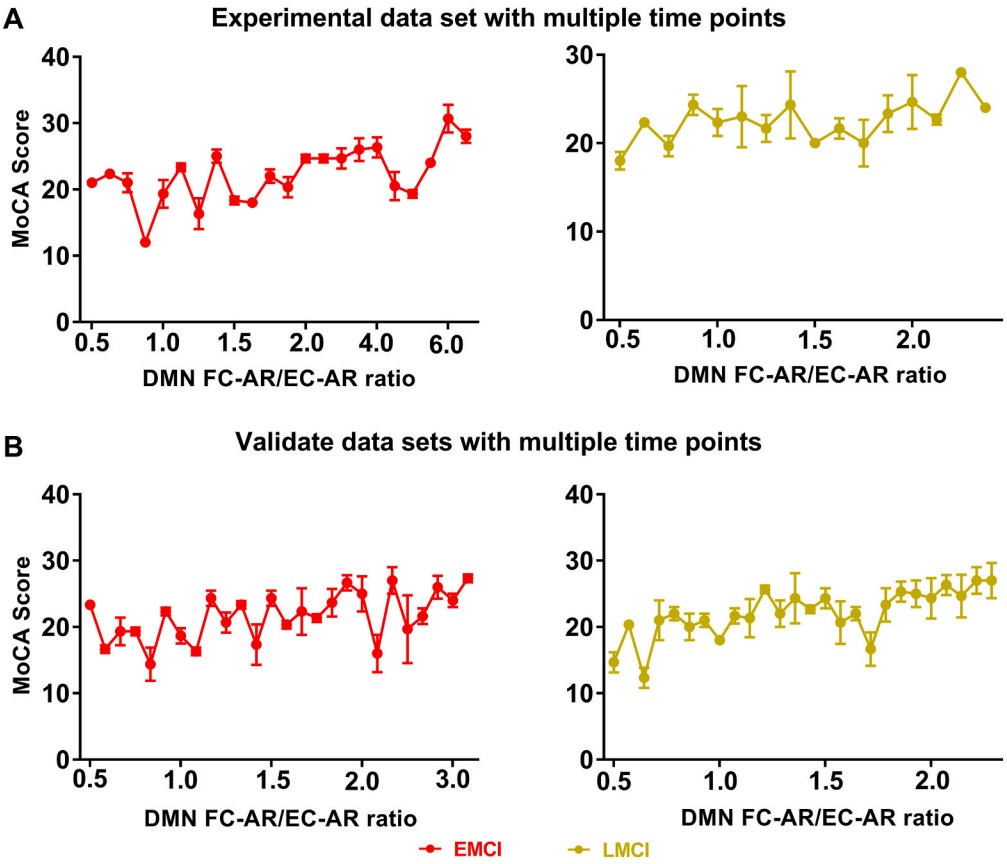

Fig. 9. The changing pattern of MoCA scores at multiple time points (DMN). (A) Experimental dataset. (B) Validation dataset.

scores. As can be seen from the results in Fig. 8A and B, there is a significant correlation between the FC-AR/EC-AR values of the DMN network module and the MoCA scores, but this correlation is gradually weakening with the development of dementia, and the results of the experimental and validation datasets largely follow this pattern.

The cerebral cortex contains a large number of synaptic structures that play an important role in the transmission of neural information and the functional synergy between different brain regions, and this process is inevitably accompanied by glucose metabolism [30]. The brain performs complex cognitive functions that require the coordinated action of many neurons across multiple brain regions. Energy signal exchange and transmission between neurons supports information communication in the brain and enhances synaptic plasticity, an important mechanism for activity [31], behavior and cognitive function [32].

This study found that some subjects in the LMCI and AD groups had higher cognitive performance scores and higher FC-AR/EC-AR values than those in the EMCI group, but overall glucose metabolism levels showed the opposite trend. Some individuals have a greater immune response that clears toxic proteins from their brains to maintain brain health in the early stages of mild cognitive impairment. In contrast, excessive immune responses may result in massive apoptosis of neurons and elevated metabolism, resulting in cognitive decline. Consequently, some individuals in the EMCI group had metabolic levels comparable to those of the normal group, but their cognitive performance scores are lower. Other individuals in the LMCI or AD groups with relatively moderate immune responses maintained better cognitive performance with synaptic potential compensation. In spite of their lower metabolic rates, the strength of the immune response may be influenced by genetic factors, and further investigation is required [33].

A significant increase in functional connectivity (FC) between brain modules implies reduced segregation between individual functional networks, whereas insignificant differentiation between network modules indicates disruption of the brain network system. The decrease in EC represents diminished coherence between FDG SUVR and ALFF values in various brain regions. This may be influenced by immune responses [33] and synaptic compensatory effects [34], suggesting altered homeostasis in the brain. Higher FC/EC values imply damage to brain networks. The FC-AR values denote the strength of connectivity between network modules and can indicate the degree of separation of each network module, the level of separation and cognitive ability have a certain correlation [23]. A greater degree of separation of network modules may also be beneficial in inhibiting the diffusion of amyloid and tau proteins in the brain, contributing to the protection of human cognitive abilities [35,36]. The FC-AR/EC-AR values presented in this study incorporate changes in the level of glucose metabolism and low-frequency signal amplitude, and both changes can, to some extent, indicate the ability of neuronal synapses to transmit information at the individual level, which is closely related to the level of cognition. When individuals experience early cognitive impairment, synaptic damage leads to a decrease in ALFF values, with a

corresponding weakening of glucose metabolism. However, due to synaptic plasticity, the activity of some neurons is enhanced and the corresponding glucose metabolism is increased. The values of electrical signals may be more sensitive relative to chemical signals, which may lead to a more pronounced decrease in the amplitude of neuronal oscillations. But this phenomenon will not always exist. When dementia develops to an advanced stage, some neuronal synapses may show abnormal discharge, but the level of neuronal metabolism in the whole brain is already at a relatively low level. Granule cells can partially compensate for the loss of synapses during aging by increasing the electrical response to synaptic activation and possibly synaptic potency [34]. Compensatory changes in synaptic strength in AD patients are also detected in axospinous synapses of the proximal and distal dendrites. Their multiple synaptic buttons may be stronger than those of the healthy group. These findings suggest that the development of AD is a multi-dimensional fusion of neurodegenerative and neuroplastic processes [37]. The investigation of its metabolic compensatory mechanisms can help to understand the pathology of AD. There is some evidence that the APOEε4 gene may confer some advantage, and that APOEε4 carriers also recall locations more precisely and have a greater advantages with higher levels of **β**-amyloid. These results suggested that there is evidence for superior visual working memory in APOEε4 gene carriers [38].

There are some limitations that need to be noted. First, although this study is based on multimodal data, it still has the potential to integrate more dimensions of information [13], for example, the relationship between FC-AR/EC-AR values and toxic proteins by combining molecular imaging data of amyloid and tau proteins to further explore the development of Alzheimer's disease and the causes of toxic protein accumulation. Second, this study has preliminarily explored the imaging features corresponding to neuronal compensatory effects and cognitive recovery phenomena, and the next step could be to investigate the genetic patterns of these imaging features, such as single-locus associations of single nucleotide polymorphisms and multi-locus interactions, which are important for the early diagnosis and prevention of Alzheimer's disease. Third, the sequence repetition time (TR) of the fMRI image data used in this study is 3 ms, and it is worth exploring and verifying whether the use of data with shorter TR times could reduce the effects of respiration and heartbeat and thus yield more accurate results.

5. Conclusions

The current research suggests that FC-AR/EC-AR values for DMN network modules may be a more accurate indicator to predict individual cognitive ability. Individuals with lower global connectivity of brain network modules and higher energy connectivity have better cognitive abilities. The evaluation index (FC-AR/EC-AR values) can measure the dissociation between the segregation of brain network modules and the energy transfer capacity of neurons, and takes into account the influence of synaptic compensatory effects on cognitive changes, incorporating more dimensions of information, which may become a more effective clinical evaluation index, and is more important for studying the pathological process of Alzheimer's disease.

Author contribution statement

Jinhua Sheng: Conceived and designed the experiments; Contributed reagents, materials, analysis tools or data; Wrote the paper.
Ze Yang: Performed the experiments; Analyzed and interpreted the data; Wrote the paper.
Qiao Zhang: Conceived and designed the experiments.
Luyun Wang, and Yu Xin: Analyzed and interpreted the data.

Ethics approval

This study was approved by the Institutional Review Board (IRB) at Hangzhou Dianzi University (IRB-2020001) and the Ethics Committee at Beijing Hospital (2022BJYYEC-375-01).

Funding statement

This work was supported by the National Natural Science Foundation of China (grant number: 62271177).

Data availability statement

All key datasets generated and analyzed during this study are included in this manuscript. The raw data are also available on reasonable request.

Additional information

No additional information is available for this paper.

Declaration of competing interest

The authors declare that they have no known competing financial interests or personal relationships that could have appeared to influence the work reported in this paper.

Appendix A. Supplementary data

Supplementary data to this article can be found online at https://doi.org/10.1016/j.heliyon.2023.e18121.

References

[1] M.R. Brier, J.B. Thomas, A.Z. Snyder, T.L. Benzinger, D. Zhang, M.E. Raichle, et al., Loss of intranetwork and internetwork resting state functional connections with Alzheimer's disease progression, J. Neurosci. 32 (2012) 8890–8899.
[2] B.T. Yeo, F.M. Krienen, J. Sepulcre, M.R. Sabuncu, D. Lashkari, M. Hollinshead, et al., The organization of the human cerebral cortex estimated by intrinsic functional connectivity, J. Neurophysiol. 106 (2011) 1125–1165.
[3] M. Scherr, L. Utz, M. Tahmasian, L. Pasquini, M.J. Grothe, J.P. Rauschecker, et al., Effective connectivity in the default mode network is distinctively disrupted in Alzheimer's disease—a simultaneous resting-state FDG-PET/fMRI study, Hum. Brain Mapp. 42 (2021) 4134–4143.
[4] C. Li, Y. Li, L. Zheng, X. Zhu, B. Shao, G. Fan, et al., Abnormal brain network connectivity in a triple-network model of Alzheimer's disease, J. Alzheim. Dis. 69 (2019) 237–252.
[5] O. Coskuner, V.N. Uversky, Intrinsically disordered proteins in various hypotheses on the pathogenesis of Alzheimer's and Parkinson's diseases, Prog. Mol. Biol. Trans. Sci. 166 (2019) 145–223.
[6] S.D. Hettiarachchi, Y. Zhou, E. Seven, M.K. Lakshmana, A.K. Kaushik, H.S. Chand, et al., Nanoparticle-mediated approaches for Alzheimer's disease pathogenesis, diagnosis, and therapeutics, J. Contr. Release 314 (2019) 125–140.
[7] P.J. Nestor, P. Scheltens, J.R. Hodges, Advances in the early detection of Alzheimer's disease, Nat. Med. 10 (2004) S34–S41.
[8] K. Mevel, B. Desgranges, J.-C. Baron, B. Landeau, V. De la Sayette, F. Viader, et al., Detecting hippocampal hypometabolism in Mild Cognitive Impairment using automatic voxel-based approaches, Neuroimage 37 (2007) 18–25.
[9] P. Manza, C.E. Wiers, E. Shokri-Kojori, D. Kroll, D. Feldman, M. Schwandt, et al., Brain network segregation and glucose energy utilization: relevance for age-related differences in cognitive function, Cerebr. Cortex 30 (2020) 5930–5942.
[10] G.S. Wig, Segregated systems of human brain networks, Trends Cognit. Sci. 21 (2017) 981–996.
[11] M. Ewers, Y. Luan, L. Frontzkowski, J. Neitzel, A. Rubinski, M. Dichgans, et al., Segregation of functional networks is associated with cognitive resilience in Alzheimer's disease, Brain 144 (2021) 2176–2185.
[12] E.M. Arenaza-Urquijo, S.A. Przybelski, T.L. Lesnick, J. Graff-Radford, M.M. Machulda, D.S. Knopman, et al., The metabolic brain signature of cognitive resilience in the 80+: beyond Alzheimer pathologies, Brain 142 (2019) 1134–1147.
[13] C. Ding, W. Du, Q. Zhang, L. Wang, Y. Han, J. Jiang, Coupling relationship between glucose and oxygen metabolisms to differentiate preclinical Alzheimer's disease and normal individuals, Hum. Brain Mapp. 42 (2021) 5051–5062.
[14] B. Kim, S.E. Elzinga, R.E. Henn, L.M. McGinley, E.L. Feldman, The effects of insulin and insulin-like growth factor I on amyloid precursor protein phosphorylation in in vitro and in vivo models of Alzheimer's disease, Neurobiol. Dis. 132 (2019), 104541.
[15] D.N. Greve, C. Svarer, P.M. Fisher, L. Feng, A.E. Hansen, W. Baare, et al., Cortical surface-based analysis reduces bias and variance in kinetic modeling of brain PET data, Neuroimage 92 (2014) 225–236.
[16] M. Richardson, K. Friston, S. Sisodiya, M. Koepp, J. Ashburner, S. Free, et al., Cortical grey matter and benzodiazepine receptors in malformations of cortical development. A voxel-based comparison of structural and functional imaging data, Brain: J. Neurol. 120 (1997) 1961–1973.
[17] N. Villain, B. Desgranges, F. Viader, V. De La Sayette, F. Mézenge, B. Landeau, et al., Relationships between hippocampal atrophy, white matter disruption, and gray matter hypometabolism in Alzheimer's disease, J. Neurosci. 28 (2008) 6174–6181.
[18] M. Zhang, W. Sun, Z. Guan, J. Hu, B. Li, G. Ye, et al., Simultaneous PET/fMRI detects distinctive alterations in functional connectivity and glucose metabolism of precuneus subregions in Alzheimer's disease, Front. Aging Neurosci. 13 (2021), 737002.
[19] M. Boccardi, M.P. Laakso, L. Bresciani, S. Galluzzi, C. Geroldi, A. Beltramello, et al., The MRI pattern of frontal and temporal brain atrophy in fronto-temporal dementia, Neurobiol. Aging 24 (2003) 95–103.
[20] C.R. Jack Jr., V.J. Lowe, M.L. Senjem, S.D. Weigand, B.J. Kemp, M.M. Shiung, et al., 11C PiB and structural MRI provide complementary information in imaging of Alzheimer's disease and amnestic mild cognitive impairment, Brain 131 (2008) 665–680.
[21] R. Ossenkoppele, B.I. Cohn-Sheehy, R. La Joie, J.W. Vogel, C. Möller, M. Lehmann, et al., Atrophy patterns in early clinical stages across distinct phenotypes of Alzheimer's disease, Hum. Brain Mapp. 36 (2015) 4421–4437.
[22] D.C. Perry, J.A. Brown, K.L. Possin, S. Datta, A. Trujillo, A. Radke, et al., Clinicopathological correlations in behavioural variant frontotemporal dementia, Brain 140 (2017) 3329–3345.
[23] M. Zhang, Z. Guan, Y. Zhang, W. Sun, W. Li, J. Hu, et al., Disrupted coupling between salience network segregation and glucose metabolism is associated with cognitive decline in Alzheimer's disease–A simultaneous resting-state FDG-PET/fMRI study, Neuroimage: Clinical 34 (2022), 102977.
[24] V. Menon, Large-scale brain networks and psychopathology: a unifying triple network model, Trends Cognit. Sci. 15 (2011) 483–506.
[25] G.M. McKhann, D.S. Knopman, H. Chertkow, B.T. Hyman, C.R. Jack Jr., C.H. Kawas, et al., The diagnosis of dementia due to Alzheimer's disease: recommendations from the National Institute on Aging-Alzheimer's Association workgroups on diagnostic guidelines for Alzheimer's disease, Alzheimer's Dementia 7 (2011) 263–269.
[26] S. Maleki Balajoo, F. Rahmani, R. Khosrowabadi, C. Meng, S.B. Eickhoff, T. Grimmer, et al., Decoupling of regional neural activity and inter-regional functional connectivity in Alzheimer's disease: a simultaneous PET/MR study, Eur. J. Nucl. Med. Mol. Imag. 49 (2022) 3173–3185.
[27] C.B. Malpas, M.M. Saling, D. Velakoulis, P. Desmond, R.J. Hicks, H. Zetterberg, et al., Cerebrospinal fluid biomarkers are differentially related to structural and functional changes in dementia of the Alzheimer's type, J. Alzheim. Dis. 62 (2018) 417–427.
[28] B.A. Gordon, T.M. Blazey, Y. Su, A. Hari-Raj, A. Dincer, S. Flores, et al., Spatial patterns of neuroimaging biomarker change in individuals from families with autosomal dominant Alzheimer's disease: a longitudinal study, Lancet Neurol. 17 (2018) 241–250.
[29] M. Scherr, L. Pasquini, G. Benson, R. Nuttall, M. Gruber, J. Neitzel, et al., Decoupling of local metabolic activity and functional connectivity links to amyloid in Alzheimer's disease, J. Alzheim. Dis. 64 (2018) 405–415.
[30] Y. Liu, C. Yu, X. Zhang, J. Liu, Y. Duan, A.F. Alexander-Bloch, et al., Impaired long distance functional connectivity and weighted network architecture in Alzheimer's disease, Cerebr. Cortex 24 (2014) 1422–1435.
[31] J. Fell, N. Axmacher, The role of phase synchronization in memory processes, Nat. Rev. Neurosci. 12 (2011) 105–118.
[32] J. Gallinat, D. Kunz, D. Senkowski, T. Kienast, F. Seifert, F. Schubert, et al., Hippocampal glutamate concentration predicts cerebral theta oscillations during cognitive processing, Psychopharmacology 187 (2006) 103–111.
[33] L. Zhao, CD33 in Alzheimer's disease–biology, pathogenesis, and therapeutics: a mini-review, Gerontology 65 (2019) 323–331.
[34] C.A. Barnes, B.L. McNAUGHTON, Physiological compensation for loss of afferent synapses in rat hippocampal granule cells during senescence, J. Physiol. 309 (1980) 473–485.
[35] H.-R. Kim, P. Lee, S.W. Seo, J.H. Roh, M. Oh, J.S. Oh, et al., Comparison of Amyloid β and tau spread models in Alzheimer's disease, Cerebr. Cortex 29 (2019) 4291–4302.

[36] N. Franzmeier, J. Neitzel, A. Rubinski, R. Smith, O. Strandberg, R. Ossenkoppele, et al., Functional brain architecture is associated with the rate of tau accumulation in Alzheimer's disease, Nat. Commun. 11 (2020) 347.
[37] K.M. Neuman, E. Molina-Campos, T.F. Musial, A.L. Price, K.-J. Oh, M.L. Wolke, et al., Evidence for Alzheimer's disease-linked synapse loss and compensation in mouse and human hippocampal CA1 pyramidal neurons, Brain Struct. Funct. 220 (2015) 3143–3165.
[38] K. Lu, J.M. Nicholas, Y. Pertzov, J. Grogan, M. Husain, I.M. Pavisic, et al., Dissociable effects of APOE ε4 and β-amyloid pathology on visual working memory, Nat. Aging 1 (2021) 1002–1009.